

instability. Acoustic liners used in combustors selectively absorb certain frequency components that can alter wave shape. They may be most effective when they remove the second harmonic component of the basic oscillation.

### References

- <sup>1</sup> Heidmann, M. F. and Wieber, P. R., "Analysis of Frequency Response Characteristics of Propellant Vaporization," TN D-3749, 1966, NASA.
- <sup>2</sup> Crocco, L. et al., "Nonlinear Aspects of Combustion Instability in Liquid Propellant Rocket Motors," AMS-SR-553g, NASA CR-72270, June 1967, Princeton Univ., Princeton, N.J.
- <sup>3</sup> Priem, R. J. and Guentert, D. C., "Combustion Instability Limits Determined by a Nonlinear Theory and a One-Dimensional Model," TN D-1409, 1962, NASA.
- <sup>4</sup> Heidmann, M. F., "Empirical Characterization of Some Pressure Wave Shapes in Strong Traveling Transverse Acoustic Modes," TM X-1716, 1969, NASA.
- <sup>5</sup> Wanhainen, J. P., Feiler, C. E., and Morgan, C. J., "Effect of Chamber Pressure, Flow per Element, and Contraction Ratio on Acoustic-Mode Instability in Hydrogen-Oxygen Rockets," TN D-4733, 1968, NASA.

## Transient Axisymmetric Bending Stress in an Infinite Cylindrical Shell at an Elastic Ring Stiffener

D. B. LONGCOPE\* AND M. J. FORRESTAL†  
Sandia Laboratories, Albuquerque, N. Mex.

**A**N infinite, circular cylindrical shell containing an internal elastic stiffener ring is subjected to an axisymmetric, uniform, radial impulse. The bending stress in the cylindrical shell at the ring stiffener is calculated from the shell bending theory which neglects transverse shear deformation and rotary inertia. In Ref. 1, bending stresses for the special case where the stiffener ring was rigid were calculated on the basis of the shell bending theory and a shell theory, which included corrections for rotary inertia and transverse shear deformation. A comparison of the response data indicated that the effects of rotary inertia and shear deformation only influenced the very early time response, and that the shell bending theory was adequate for predicting the maximum bending stress.

### Equations of Motion

For the circular cylindrical shell shown in cross section in Fig. 1, the equation of motion according to the shell bending theory, with the axial normal stress resultant taken as zero, is

$$(\partial^4 W / \partial X^4) + \alpha^2 [W + (\partial^2 W / \partial T^2)] = (\alpha^2 c I / E h) \delta(T) \quad (1a)$$

$$W = w/a; X = x/a; T = ct/a; c^2 = E/\rho; \alpha^2 =$$

$$[12(1 - \nu^2)a^2]/h^2 \quad (1b)$$

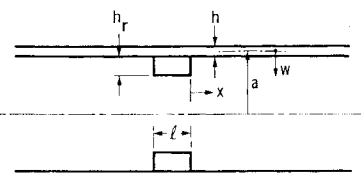


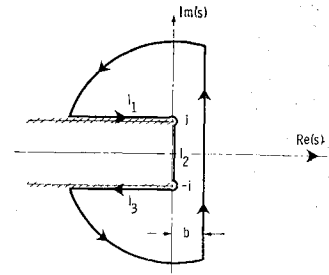
Fig. 1 Geometry of the problem.

Received September 14, 1970; revision received October 26, 1970. This work was supported by the U.S. Atomic Energy Commission.

\* Staff Member, Exploratory Systems Development Department.

† Division Supervisor, Shock Simulation Department. Associate Fellow AIAA.

Fig. 2 Path of integration.



where  $w$  is the radial shell displacement;  $x$  is the axial coordinate;  $t$  is time;  $I$  is the specific impulse;  $\delta(T)$  is the Dirac delta function; and  $a$ ,  $h$ ,  $\rho$ ,  $E$ , and  $\nu$  are the shell radius, thickness, density, Young's modulus, and Poisson's ratio, respectively.

The shell is infinite in either direction from the ring support, and the following boundary conditions for the shell are taken at the support

$$\partial W / \partial X = 0 \quad \text{at } X = 0 \quad (2a)$$

$$\frac{\partial^3 W}{\partial X^3} + \frac{\alpha^2 L}{2} \left[ (1 + nK)W + (1 + nM) \frac{\partial^2 W}{\partial T^2} \right] = \frac{\alpha^2 c I L}{2 E h} \delta(T) \quad \text{at } X = 0 \quad (2b)$$

where

$$n = h_r/h; K = E_r/E; M = \rho_r/\rho; L = l/a \quad (2c)$$

and  $l$ ,  $h_r$ ,  $\rho_r$ , and  $E_r$  are the ring length, thickness, density, and Young's modulus, respectively. Symmetry requires that the slope of the shell vanishes at the ring stiffener and Eq. (2b) requires that the ring and shell displacements are equal at the ring-shell interface. It is assumed in the development of Eq. (2b) that the ring radius is equal to the shell radius  $a$ . Equation (2b) is essentially the equation of motion for a ring that includes the resistance of the shear forces of the shell; this is accounted for by the term  $\partial^3 W / \partial X^3$ . These shell boundary conditions are the same as those given in Ref. 2.

### Solution

The bending stress in the shell at the ring stiffener is obtained by employing the Laplace transform method. The transform of Eq. (1a) with quiescent initial conditions is

$$\partial^4 \bar{W} / \partial X^4 + \alpha^2 (1 + s^2) \bar{W} = \alpha^2 c I / E h \quad (3)$$

where  $\bar{W}$  is the transform of  $W$ , and  $s$  is the transform variable. The transformed bending stress at the radially outer shell surface is given by

$$\bar{\sigma}_x^* = [E h / 2a(1 - \nu^2)] \partial^2 \bar{W} / \partial X^2 \quad (4)$$

Equation (3) is solved subject to Eqs. (2a) and (2b) and the requirement that  $\bar{W}$  is bounded as  $X \rightarrow \infty$ . The solution  $\bar{W}$  is substituted into Eq. (4) and evaluated at  $X = 0$  to give

$$\bar{\sigma}_x^* = \frac{\alpha c I n M (a_0 + s^2)}{2a(1 - \nu^2)(1 + nM)(1 + s^2)^{1/2} [b_0 + b_1(1 + s^2)^{3/4} + s^2]} \quad (5a)$$

$$a_0 = K/M; b_0 = 1 + nK/1 + nM; b_1 = 2^{3/2} / \alpha^{1/2} L (1 + nM) \quad (5b)$$

Thus the formal solution for the bending stress at the outer shell surface for  $X = 0$  is

$$\sigma_x^* = \frac{1}{2\pi i} \int_{b-i\infty}^{b+i\infty} e^{sT} \bar{\sigma}_x^* ds \quad (6)$$

where  $b$  is a real, positive number.

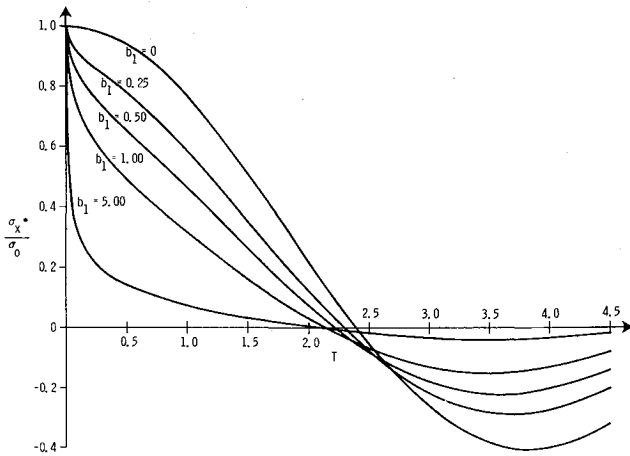


Fig. 3 Bending stress at the radially outward shell surface for  $X = 0$ .

Equation (6) is evaluated by considering the contour and branch cuts shown in Fig. 2. Utilizing Cauchy's theorem, the formal integral solution is replaced by the contributions of the poles of the integrand within the contour and the line integrals along  $l_1$ ,  $l_2$ , and  $l_3$ . In general, the integrand has a pole at each of the two points where  $F(s) = b_0 + b_1(1 + s^2)^{3/4} + s^2 = 0$ . For  $b_0 < 1$ , a detailed analysis of  $F(s)$  indicates that two complex conjugate poles are located on the imaginary axis within  $|Im(s)| < 1$ . When  $b_0 > 1$ , the theorem of the argument<sup>3</sup> can be used to show that the two poles are located in the  $s$  plane where  $Re(s) < 0$  and  $|Im(s)| > 1$ , simultaneously.

However, for the interesting case where the ring and shell are of the same material  $b_0 = a_0 = 1$ , and the transformed solution reduces to

$$\bar{\sigma}_x^*/\sigma_0 = 1/(1 + s^2)^{1/4}[b_1 + (1 + s^2)^{1/4}] \quad (7a)$$

$$\sigma_0 = 3^{1/2}cI/(1 - \nu^2)^{1/2}h(1 + 1/n); \quad b_1 = 2^{3/2}/\alpha^{1/2}L(1 + n) \quad (7b)$$

The integrand given by Eq. (7a) has no poles and the bending stress  $\sigma_x^*$  at the outer shell surface for  $X = 0$  is given by

$$\frac{\sigma_x^*}{\sigma_0} = -\frac{1}{\pi} \int_0^\infty \times \frac{e^{-uT}[(b_1 + \rho \cos \alpha) \sin(T - \alpha) - \rho \sin \alpha \cos(T - \alpha)]}{\rho(b_1^2 + 2b_1\rho \cos \alpha + \rho^2)} du + \frac{1}{\pi} \int_0^1 \frac{\cos uT}{(1 - u^2)^{1/4}[b_1 + (1 - u^2)^{1/4}]} du \quad (8a)$$

$$\rho = u^{1/4}(4 + u^2)^{1/8}; \quad \alpha = 3\pi/8 + \psi/4; \quad \psi = \cos^{-1}[2/(4 + u^2)^{1/2}] \quad (8b)$$

In Eq. (8a), the first integral is the contribution along  $l_1$  and  $l_3$  and the second integral is the contribution along  $l_2$ . The integrals in Eq. (8a) can be made proper by the substitution  $u = v^2$  in the first integral and  $u = 1 - v^2$  in the second integral.

### Numerical Results

Equation (8a) was evaluated numerically for several values of the parameter  $b_1$ . Figure 3 shows the bending stress history in the outer shell fibers at the ring support for the case where the ring and shell materials are the same and  $b_1 = 0, 0.25, 0.50, 1.00$ , and  $5.00$ . The bending stresses asymptotically approach zero for large values of time. Decreasing values of  $b_1$  correspond to the ring becoming more massive relative to the shell. From Ref. 1, for a clamped boundary condition at  $X = 0$ , the bending stress at  $T = 0$  is  $\sigma_x^* = 3^{1/2}cI/[(1 - \nu^2)h]$ ; therefore, for an elastic ring, the bending stress at  $X = T = 0$  is reduced by the factor  $1/(1 + h/h_r)$ .

### References

- <sup>1</sup> Sagartz, M. J. and Forrestal, M. J., "Transient Stresses at a Clamped Support of a Circular Cylindrical Shell," *Journal of Applied Mechanics*, Vol. 36, No. 2, June 1969, pp. 367-369.
- <sup>2</sup> Baron, M. L., "Circular-Symmetric Vibrations of Infinitely Long Cylindrical Shells with Equidistant Stiffeners," *Journal of Applied Mechanics*, Vol. 23, No. 2, June 1956, pp. 316-318.
- <sup>3</sup> Kaplan, W., *Operational Methods for Linear Systems*, Addison-Wesley, Reading, Mass., 1962, pp. 156-158.

## Vortex Shedding from Circular Cylinders in an Oscillating Freestream

C. F. CHEN\* AND DAVID B. BALLENGEE†  
Rutgers University, New Brunswick, N. J.

### I. Introduction

VORTEX shedding (i.e., from smoke stacks, missiles erected on the launch pad, and tall buildings) due to atmospheric wind is a complicated phenomenon because a) the flow is sheared in the atmospheric boundary layer, b) the flow is generally unsteady, and c) there are three-dimensional effects due to finite height. The effect of flow shear on vortex shedding from circular cylinders has been investigated by Chen and Mangione<sup>1</sup> for a Reynolds number range of 200 to 800. The results show that the local Strouhal and Reynolds numbers, in which characteristic velocity is that of the local approaching stream, correlate in much the same manner as those found for uniform flow. Recently we have concluded a series of experiments on vortex shedding from circular cylinders in an oscillating free stream. The Reynolds number range tested was from 500 to  $4 \times 10^4$ , and the frequencies of oscillation were 3 and 6 Hz. The experimental procedure and results are summarized below.

### II. Experimental Apparatus and Procedure

A sketch of the wind tunnel used is shown in Fig. 1. The prime mover is an air-to-air ejector using high-pressure air at 125 psig. A muffler box is placed around the secondary air inlet and it is lined with acoustical insulation to reduce the noise level. Oscillation of the freestream is obtained by a butterfly valve placed downstream of the primary air nozzle.

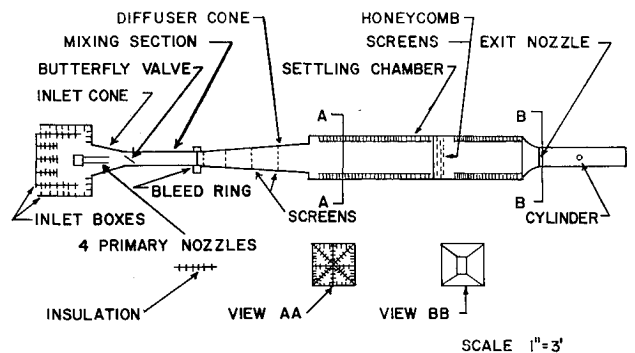


Fig. 1 Sketch of the oscillating flow wind tunnel.

Received September 16, 1970; revision received October 19, 1970. Research sponsored by AFOSR, Office of Aerospace Research, United States Air Force, under Contract F 44620-68-C-0018, monitored by D. L. Calvert.

\* Professor of Aerospace Engineering. Member AIAA.

† Research Assistant, Department of Mechanical & Aerospace Engineering; now at Jersey Central Power and Light Company, Parsippany, N. J.